AIAA AVIATION Forum
June 25-29, 2018, Atlanta, Georgia
2018 AIAA/CEAS Aeroacoustics Conference

10.2514/6.2018-3291

Deconvolution of the wavenumber - frequency spectra of wall pressure fluctuations

Simon L. Prigent*, Rafael Engelman†, Édouard Salze ‡, and Christophe Bailly§
Univ Lyon, Ecole Centrale de Lyon and LMFA UMR CNRS 5509, Ecully, France, F-69134

The wavenumber - frequency spectra of a pressure field beneath a turbulent boundary layer is considered, with the aim of removing the effect of the measuring device. A rotating antenna of aligned microphones has been used in previous studies and the measured spectra are shown to be a convolution of the true spectra with the transfer function of said antenna. Deconvolution algorithms are presented that were previously developed for other fields of studies. Test cases and processing of experimental data show that until a better convergence criteria is defined for the iterative process, a hybrid approach between deconvolution and angular interpolation of the antenna's rotation could be the best compromise.

p			=	wall pressure fluctuations
$\hat{p}$			=	frequency Fourier transform of the wall pressure fluctuations
$\tilde{p}$			=	wavenumber - frequency Fourier transform of the wall pressure fluctuations
Φ_{pp}			=	wavenumber frequency spectra of the wall pressure fluctuations
R_{pp}			=	cross spectral density of the wall pressure fluctuations
$\tilde{h}$			=	transfer function of the antenna's geometry, also referred to as convolution function
$\mathcal{F}$			=	Fourier transform operator
$\mathcal{S}_s$	$\mathcal{S}_f$	$\mathcal{S}_m$	=	un-biased and reconstructed Fourier spaces, and measurement space, respectively.
$\bullet_s$	$\bullet_f$	$\bullet_m$	=	subscripts for elements of $\mathcal{S}_s$, $\mathcal{S}_f$ and $\mathcal{S}_m$.

Introduction

The interest in wall pressure fluctuations goes back several decades [1, 2] as it is key to understanding structural vibrations and vibro-acoustics issues in applications ranging from hydrodynamics to aeronautics as well as rail or automotive industries. These fluctuations can be divided into the acoustic and hydrodynamic components, the former being induced by acoustic waves impacting onto the wall, and the latter directly by the turbulent boundary layer. The simultaneous study of both components is an experimental challenge, due to the large range of scales involved. In fact, most studies have focused on the hydrodynamic components and tried to offer a model for their spectra, such as that by Corcos [3]. However, the acoustic components, while of much lower amplitude, can play an important role for internal noise as it is commonly associated with radiating modes. Recent studies by Arguillat *et al.* [4] and Salze *et al.* [5, 6] have offered a mean to separate the two components from experimental measurements of a wall pressure field beneath a turbulent boundary layer. The authors have developed rotating antennas of microphones which allow the computation of the wavenumber - frequency spectra of the fluctuations, and offer a means to study both components separately for sufficiently high frequencies and/or Reynolds number.

As detailed by Salze *et al.* [5, 6], such an antenna consists of a non-equidistant array of microphones that simultaneously record data to compute cross-spectra. Rotating the antenna with regards to the flow direction increases the number of different separation vectors that can be obtained through combination of all microphone positions. Assuming homogeneity of the wall pressure field, the authors were able to use the large amount of separation vectors to perform a spatial Fourier transform of the cross-spectra, which gives the wavenumber - frequency spectra. The latter thus depends on the number of separation vectors, and their values, that is to say they depend on the geometry of the antenna.

*Post-doctoral fellow
†MSc student, Faculty of Mechanical and Industrial Engineering, TU WIEN
‡Research engineer
§Professor, AIAA senior member

In the field of beamforming, the use of deconvolution to recover the acoustic source maps from data biased by the geometry of a microphone array has been the topic of many studies [7–9], with the most commonly used algorithm being DAMAS2, introduced by Dougherty [10]. In particular, Ehrenfried and Koop[7] provided a detailed study on the application of such methods.

The use of the wavenumber-frequency spectra, however, is less common. Bahr and Cattafesta [11] have used this formalism to introduce a method of deconvolution of arbitrarily coherent acoustic sources, using a wavenumber-frequency covariance as an intermediate step in their algorithm. Some studies by Haxter and Spehr [12], and Erenfield and Koop [13] have looked directly into wavenumber-frequency spectra not as a means but as experimental data and have applied deconvolution to try and recover un-biased data. However, to the authors knowledge, there is still a number of uncertainties as to how to apply such deconvolution to wavenumber-frequency spectra, and more details on parameters used in the algorithm itself is much needed.

The aim of this study is thus to investigate the applicability of common deconvolution algorithms, particularly DAMAS2, to the case of the wavenumber-frequency spectra of wall pressure fluctuations beneath a turbulent boundary layer, measured by a rotating antenna such as that of Salze *et al.* [5, 6]. A particular focus will be put on practical issues that can arise.

Convolution

The wavenumber - frequency transform

Physically speaking, there exists a pressure field $p(\boldsymbol{x}, t)$, which has a wavenumber-frequency transform $\tilde{p}_s$ that can be defined in a $\boldsymbol{k}_s - \omega$ space referred to as the source space $\mathcal{S}_s$. The antenna of microphones samples this data from specific physical-space positions, to be processed as time Fourier transforms $\hat{p}$. This measurement space $\mathcal{S}_m$ is thus set in terms of $\boldsymbol{x} - \omega$. Once this space-frequency data is sampled, the reconstructed wavenumber-frequency transform $\tilde{p}$ can be computed and shall be expressed in terms of $\boldsymbol{k}_f - \omega$ in $\mathcal{S}_f$. The goal is thus to understand how the reconstructed transform $\tilde{p}$ is linked to the pre-existing unbiased transform $\tilde{p}_s$.

Analytically, and without the sampling constraints, the links between the mentioned transforms are expressed in terms of Fourier pairs as follows :

$$\tilde{p}(\boldsymbol{k}_f, \omega) = \frac{1}{(2\pi)^2} \int_{\mathcal{S}_m} \hat{p}(\boldsymbol{x}, \omega) e^{-i\boldsymbol{k}_f \cdot \boldsymbol{x}} \, \mathrm{d}\boldsymbol{x},$$

$$\hat{p}(\boldsymbol{x}, \omega) = \int_{\mathcal{S}_s} \tilde{p}_s(\boldsymbol{k}_s, \omega) e^{i\boldsymbol{k}_s \cdot \boldsymbol{x}} \, \mathrm{d}\boldsymbol{k}_s. \tag{1}$$

Hence

$$\begin{aligned}\tilde{p}(\boldsymbol{k}_f, \omega) &= \frac{1}{(2\pi)^2} \iint_{\mathcal{S}_m \mathcal{S}_s} \tilde{p}_s(\boldsymbol{k}_s, \omega) e^{i\boldsymbol{k}_s \cdot \boldsymbol{x}} \, \mathrm{d}\boldsymbol{k}_s \, e^{-i\boldsymbol{k}_f \cdot x} \, \mathrm{d}\boldsymbol{x} \\ &= \int_{\mathcal{S}_s} \left\{ \int_{\mathcal{S}_m} \frac{1}{(2\pi)^2} e^{-i(\boldsymbol{k}_f - \boldsymbol{k}_s) \cdot \boldsymbol{x}} \, \mathrm{d}\boldsymbol{x} \right\} \tilde{p}_s(\boldsymbol{k}_f, \omega) \, \mathrm{d}\boldsymbol{k}_s.\end{aligned}$$

The link between the source and reconstructed wavenumber-frequency transforms can thus be formulated as a convolution product:

$$\tilde{p}(\bullet, \omega) = (\tilde{p}_s \star \tilde{h})(\bullet, \omega) \quad \text{with} \quad \tilde{h}(\boldsymbol{k}) \equiv \frac{1}{(2\pi)^2} \int_{\mathcal{S}_m} e^{-i\boldsymbol{k} \cdot \boldsymbol{r}} \, \mathrm{d}\boldsymbol{r}. \tag{2}$$

In the analytical case, and assuming the measurement space goes to infinity for both components of $\boldsymbol{r}$, the function $\tilde{h}$ is equal to a Dirac distribution and one can write $\tilde{h}(\boldsymbol{k}_f - \boldsymbol{k}_s) = \delta(\boldsymbol{k}_f - \boldsymbol{k}_s)$. As a result, one obtains the relation $\tilde{p}(\bullet, \omega) = \tilde{p}_s(\bullet, \omega)$. The measurements are in fact performed with a finite number of points, set by the antenna's geometry, that will require a discretisation of Eq. (2). In that regard, the convolution function $\tilde{h}$ is not a Dirac distribution any more, and becomes the transfer function of the antenna's geometry.

The wavenumber - frequency spectra

The convolution product set for $\tilde{p}$ is of interest to understand the approach and write down some of the equations that will be used later on. However, it is important to realise that the wavenumber-frequency spectral density is not directly obtained from the wavenumber-frequency transform. The wavenumber-frequency spectra Φ_{pp} is defined as:

$$\Phi_{pp}(\boldsymbol{k},\omega) \equiv \frac{1}{(2\pi)^2} \int_{\mathcal{S}_m} R_{pp}(\boldsymbol{r},\omega) e^{-i\boldsymbol{k}\cdot\boldsymbol{r}} \, \mathrm{d}\boldsymbol{r} \tag{3}$$

where the cross-spectral density of the wall pressure fluctuations R_{pp} is calculated as

$$R_{pp}(\boldsymbol{x},\boldsymbol{r},\omega) \equiv \lim_{T\to\infty} \frac{2\pi}{T} E[\hat{p}(\boldsymbol{x},\omega)\hat{p}^*(\boldsymbol{x}+\boldsymbol{r},\omega)]$$

for broadband signals, and assuming $R_{pp}(\boldsymbol{x},\boldsymbol{r},\omega) = R_{pp}(\boldsymbol{r},\omega)$ for homogeneous wall pressure field. The operators lim and E being linear here, we shall consider the following quantity:

$$T(\boldsymbol{k},\omega) = \int_{\mathcal{S}_m} \hat{p}(0,\omega)\hat{p}^*(\boldsymbol{r},\omega) e^{-i\boldsymbol{k}\cdot\boldsymbol{r}} \, \mathrm{d}\boldsymbol{r}.$$

We know from Eq. (1) that

$$\tilde{p}_s(\boldsymbol{k}_s,\omega) = \frac{1}{(2\pi)^2} \int_{\mathcal{S}_m} \hat{p}(\boldsymbol{x},\omega) e^{-i\boldsymbol{k}_s\cdot\boldsymbol{x}} \, \mathrm{d}\boldsymbol{x},$$

hence

$$\begin{aligned}
T(\boldsymbol{k}_f,\omega) &= \hat{p}(0,\omega) \int_{\mathcal{S}_m} \left(\int_{\mathcal{S}_s} \tilde{p}_s(\boldsymbol{k}_s,\omega) \, e^{i\boldsymbol{k}_s\cdot\boldsymbol{r}} \, \mathrm{d}\boldsymbol{k}_s \right)^* e^{-i\boldsymbol{k}_f\cdot\boldsymbol{r}} \, \mathrm{d}\boldsymbol{r} \\
&= \hat{p}(0,\omega) \iint_{\mathcal{S}_m \mathcal{S}_s} \tilde{p}_s^*(\boldsymbol{k}_s,\omega) \, e^{-i\boldsymbol{k}_s\cdot\boldsymbol{r}} \, \mathrm{d}\boldsymbol{k}_s \, e^{-i\boldsymbol{k}_f\cdot\boldsymbol{r}} \, \mathrm{d}\boldsymbol{r} \\
&= -\hat{p}(0,\omega) \iint_{\mathcal{S}_m \mathcal{S}_s} \tilde{p}_s^*(-\boldsymbol{k}_s,\omega) \, e^{-i(\boldsymbol{k}_f-\boldsymbol{k}_s)\cdot\boldsymbol{r}} \, \mathrm{d}\boldsymbol{k}_s \, \mathrm{d}\boldsymbol{r}
\end{aligned}$$

by the change of variable $-\boldsymbol{k}_s$ to $\boldsymbol{k}_s$. Let's now consider

$$\begin{aligned}
T_s(\boldsymbol{k}_s,\omega) &= \int_{\mathcal{S}_m} \hat{p}(0,\omega)\hat{p}^*(\boldsymbol{r},\omega) e^{-i\boldsymbol{k}_s\cdot\boldsymbol{r}} \, \mathrm{d}\boldsymbol{r} \\
&= -\hat{p}(0,\omega) \left\{ \int_{\mathcal{S}_m} \hat{p}(-\boldsymbol{r},\omega) e^{-i\boldsymbol{k}_s\cdot\boldsymbol{r}} \, \mathrm{d}\boldsymbol{r} \right\}^* \\
&= -(2\pi)^2 \hat{p}(0,\omega) \, \tilde{p}_s^*(-\boldsymbol{k}_s,\omega)
\end{aligned}$$

One has

$$\begin{aligned}
\int_{\mathcal{S}_s} T_s(\boldsymbol{k}_s,\omega)\tilde{h}(\boldsymbol{k}_f-\boldsymbol{k}_s) \, \mathrm{d}\boldsymbol{k}_s &= -\hat{p}(0,\omega) \int_{\mathcal{S}_s} \tilde{p}_s^*(-\boldsymbol{k}_s,\omega) \int_{\mathcal{S}_m} e^{-i(\boldsymbol{k}_f-\boldsymbol{k}_s)\cdot\boldsymbol{r}} \, \mathrm{d}\boldsymbol{r} \, \mathrm{d}\boldsymbol{k}_s \\
&= -\hat{p}(0,\omega) \iint_{\mathcal{S}_m \mathcal{S}_s} \tilde{p}_s^*(-\boldsymbol{k}_s,\omega) \, e^{-i(\boldsymbol{k}_f-\boldsymbol{k}_s)\cdot\boldsymbol{r}} \, \mathrm{d}\boldsymbol{k}_s \, \mathrm{d}\boldsymbol{r}
\end{aligned}$$

Thus:

$$T(\bullet, \omega) = (T_s \star \tilde{h})(\bullet, \omega)$$

The convolution problem for the wavenumber-frequency spectra is set as:

$$\Phi_{pp}(\bullet, \omega) = (\Phi_{s,pp} \star \tilde{h})(\bullet, \omega) \tag{4}$$

with $\tilde{h}$ defined in Eq. (2). It is worth noting that the transfer function $\tilde{h}$ is the same for both wavenumber-frequency spectra and transforms. At this stage, $\tilde{h}$ is known since $\boldsymbol{r}$ and $\boldsymbol{k}$ are given by the antenna's geometry and the processing scheme respectively. Φ_{pp} is measured and therefore only $\Phi_{s,pp}$ is an unknown of this convolution problem.

Discrete problem

The antenna of reference in the current study consists of 63 microphones aligned on a rotating disk, as detailed by Salze *et al.* [5, 6]. For each angular position, a separation vector $\boldsymbol{r}$ is obtained from all possible combinations of microphones and is used to calculate R_{pp} as illustrated in fig. 1.

The discrete form of the spectra and transfer function, defined in Eq.(3) and Eq.(2) is thus:

$$\Phi_{pp}(\boldsymbol{k}, \omega) = \frac{1}{(2\pi)^2} \sum_m \sum_n R_{pp}(\boldsymbol{r}_{nm}, \omega) e^{-i\boldsymbol{k}\cdot\boldsymbol{r}_{nm}} \, \mathrm{d}s_n \tag{5}$$

and

$$\tilde{h}(\boldsymbol{k}) = \frac{1}{(2\pi)^2} \sum_m \sum_n e^{-i\boldsymbol{k}\cdot\boldsymbol{r}_{nm}} \, \mathrm{d}s_n, \tag{6}$$

where $\mathrm{d}s_n$ represents the local area around the point of summation. Therefore the element $\tilde{h}_{i,j}$ corresponds to $\tilde{h}\left(\{k_x(j), k_y(i)\}\right)$ calculated with the above equation.
This discretisation is the cause of the geometric bias introduced by the antenna and that needs correcting. Note that due to the symmetry of the antenna and the assumed homogeneity of the pressure field, both $\tilde{h}$ and Φ_{pp} are real.

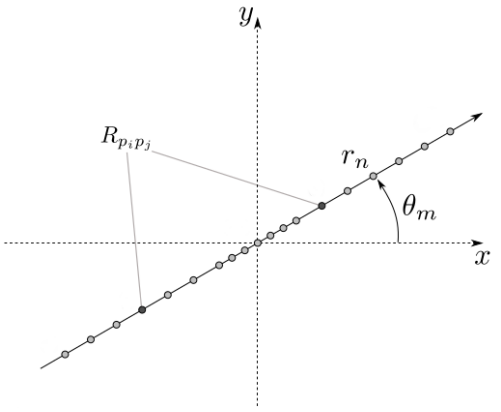

Fig. 1 Sketch of the rotating antenna: separation vector $\boldsymbol{r}$.

In his study of deconvolution techniques for beamforming, Dougherty [10] presented two methods: one based on the application of a spectral filter and the other being a new version of the common iterative deconvolution process called DAMAS. Both methods are introduced and applied to the wavenumber-frequency spectra in the following sections.

Algorithms for deconvolution

The Wiener filtering method assumes a convolution relation with noise, adding an extra term to Eq. (4), and gives a solution which minimises the error between the true $\Phi_{s,pp}$ and estimated Φ_{pp} spectra in a mean square sense [14]. This, however, requires to have information about the power spectra of the noise. An approximate solution can be given by the below equation, where the filter itself is in brackets, γ is a parameter to be set and $\mathcal{F}$ stands for the direct Fourier transform operator.

$$\Phi_{s,pp} = \left[\frac{\mathcal{F}(\tilde{h})^*}{|\mathcal{F}(\tilde{h})|^2 + \gamma} \right] \Phi_{pp}$$

Dougherty [10] has applied this method to the deconvolution of acoustic sources power maps and added a positivity constraint to remove non-physical negative values. Due to this added constraint, the author reported that it was not applicable to that case. It is worth noting though, that for the present study, no positivity constraint is required, as the spectra can have negative values. There is therefore no *a priori* reason to reject this method and it will thus be presented.

Iterative deconvolution approaches [7–9, 12] have been taken to tackle problems of acoustics sources localisation using microphone arrays, with in particular the DAMAS algorithm by Brooks and Humphreys [15, 16] and extensions such as DAMAS2 [10]. The DAMAS2 algorithm takes advantage of the convolution theorem to perform multiplication in a Fourier space instead of convolution product in the original space. The process is as follows [10]:

Initialise:

- $a = \sum_{i,j} |\tilde{h}_{i,j}|$
- $\Psi(\Upsilon_1, \Upsilon_2) = \exp\left(-\frac{\Upsilon_1^2+\Upsilon_2^2}{2\Upsilon_0^2}\right)$
- compute $\mathcal{F}(\tilde{h})$.

Iterate from n to $n+1$:

- $b^{(n)} = \mathcal{F}^{-1}\left[\mathcal{F}(\Phi_{s,pp}^{(n)})\mathcal{F}(\tilde{h})\Psi\right]$
- $\Phi_{s,pp}^{(n+1)} = \max\left(\Phi_{s,pp}^{(n)} + \frac{\Phi_{pp}-b^{(n)}}{a}, 0\right)$

Here, Υ denotes the variable in the Fourier space, and although it has the same dimension as the original (x, y) space, one should note it is not obtained via an inverse Fourier transform of the $\boldsymbol{k}$ space, but rather an additional direct Fourier transform. Ψ is a Gaussian filter with Υ_0 setting its width ; and a is a relaxation parameter.

Analytical test cases

For the purpose of testing the method and applicability of the mentioned algorithms to the wavenumber-frequency spectra of wall pressure fluctuations beneath a turbulent boundary layer, analytical test cases are taken as a combination of an acoustic diffuse field and a Corcos-like pressure field :

$$S_{dif}(\boldsymbol{\zeta}, \omega) = A\frac{\sin(k_0|\boldsymbol{\zeta}|)}{k_0|\boldsymbol{\zeta}|}$$

$$S_{cor}(\boldsymbol{\zeta}, \omega) = e^{-k_c|\zeta_1|/\alpha}e^{-k_c|\zeta_2|/\beta}e^{ik_c\zeta_1}$$

Analytical expressions of the corresponding spectra are:

$$\Phi_{dif} = \begin{cases} \frac{1}{2\pi k_0^2}\frac{1}{\sqrt{1-(|\boldsymbol{k}|/k_0)^2}} & \text{if} \quad |\boldsymbol{k}| < k_0 \\ 0 & \text{if} \quad |\boldsymbol{k}| > k_0 \end{cases}$$

$$\Phi_{cor} = \frac{A}{\pi^2}\frac{\alpha k_c}{k_c^2+\alpha^2(k_x-k_c)^2}\frac{\beta k_c}{k_c^2+\beta^2 k_y^2}$$

The array geometry that will be taken for this study is that of the rotating antenna from Salze *et al.* [5, 6]. In order to match with these previous experimental campaings, and unless stated otherwise in specific sections of this study, the following parameters were used: $f = 3750\,\text{Hz}$, $U_c = 0.7 * 75\,\text{m.s}^{-1}$, $k_c = 2 * \pi * f/U_c\,\text{m}^{-1}$, $k_0 = 2 * \pi * f/c_0\,\text{m}^{-1}$, $c_0 = \sqrt{1.4 * 286.07 * (273.15 + 20)}\,\text{m.s}^{-1}$, $\alpha = 8$, $\beta = 1$ and $A = 0.01$. Note that for the following tests, the algorithms were applied to square data matrices. For ease of visualisation, data sets are then only displayed for $-100 < k_x < 800\,\text{m}^{-1}$.

Results from the Wiener filter

In the definition of the Wiener filter presented above, the parameter γ is to be adjusted to render the deconvolution as well as possible. It is thus important to check its effect on the spectra, and to this end the synthetic data before and after deconvolution can be checked against the analytical expression of said spectra.

Fig. 2 shows $k_y = 0$ and $k_x = k_c$ profiles of the spectra for the synthetic data artificially measured with the antenna geometry, before and after deconvolution with different values of γ and the analytical profiles for comparison. It is clear that the measured spectra overestimates the value of the convective ridge, in both profiles, by around 25 %. However, and despite some oscillations, the acoustic part of the $k_y = 0$ is rather well recovered.

Once the deconvolution is applied, the convective ridge overestimate is reduced with the best fit obtained for $\gamma = 0.01$ and $\gamma = 0.001$. However, while reducing the value of γ does not seem to affect the level of the convective ridge, it clearly introduces strong oscillations, in particular in the sub-convective and acoustic regions. From these results, it seems that $\gamma = 0.01$ is the best suited value to fit the synthetic data.

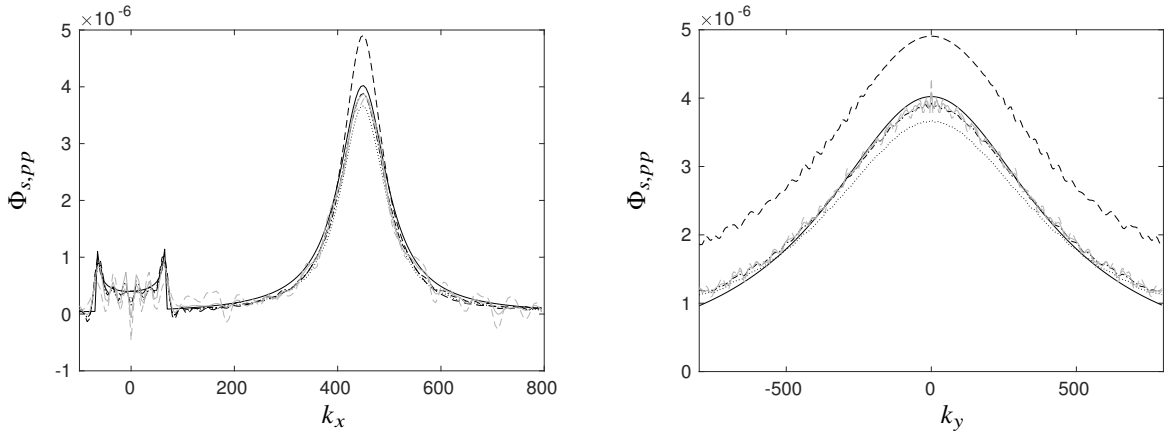

(a) $\Phi_{s,pp}$ **at** $k_y = 0$**.** **(b)** $\Phi_{s,pp}$ **at** $k_x = k_c$**.**

Fig. 2 Spectra deconvolved with Wiener filters: cross plots. ——— analytic, − − − array-sampled, ····· $\gamma = 0.1$, − · − · $\gamma = 0.01$, ——— $\gamma = 0.001$, – – – $\gamma = 0.0001$.

Fig. 3 shows the spectra before and after Wiener deconvolution with two values of γ. With $\gamma = 0.01$, the overall aspect is rather similar to the original spectra, slightly more blurry although it is less obvious than in the profiles, but the main effect is in the convective ridge as previously discussed. When using $\gamma = 0.001$, it is clear even from the spectra map that the deconvolution has made it much more noisy than the measured spectra.

Overall, a value of $\gamma = 0.01$ is the most suited to our data for the deconvolution with a Wiener filter. However, this deconvolution introduces oscillations, in particular in the acoustic region, that need to be kept in mind.

Results from DAMAS2

As mentioned before, the studies using DAMAS2 rarely go into the details of the implementation. For this reason, three questions remain open and should be addressed. First, while the transfer function $\tilde{h}$ has been formally defined it is still unclear to the authors whether it should be normalised or used as such in the algorithm. The use of a Gaussian filter during the iteration is also an important point to address. Finally, the positivity constraint applied at each iteration requires further investigation within the frame of the present study.

DAMAS2 being an iterative process, it is important to define a criteria to stop the loop. To this end, the value $\sum_{i,j} \left(\Phi_{pp} - b^{(n)}\right)/a$ from the iterative steps shall be followed; and henceforth referred to as residual.

Normalisation of $\tilde{h}$

The norm of $\tilde{h}$ is directly linked to the speed of the iterative correction in the DAMAS2 algorithm, since the relaxation parameter a is defined as $a = \sum_{i,j} |\tilde{h}_{i,j}|$. Two cases are tested in this section, first $\tilde{h}$ is left without normalisation and is simply taken from the discrete equivalent of its definition from Eq. (6). In the second case, $\tilde{h}$ is normalised by its standard Frobenius norm:

$$\tilde{h} := \tilde{h} \Big/ \left(\sum_{i,j} \tilde{h}_{i,j}^2 \right)^{1/2}.$$

Fig. 4a shows the evolution of the residual during the deconvolution for both the normalised and standard cases. In the normalised case, the amplitude of the residual decays after an initial jump, and has a minimum around 200 iterations. On the other hand, the standard case does not exhibit a local extrema ; but rather has an inflection point, that would indicate 400 to 500 iterations if it were to be taken as the criteria to stop the iterations.

To complement this observation, fig. 4b displays the sum of the spectra over all wavenumbers, that is the spectral density at the selected frequency, normalised by that of the original spectra. After a slight decay, this value of energy is

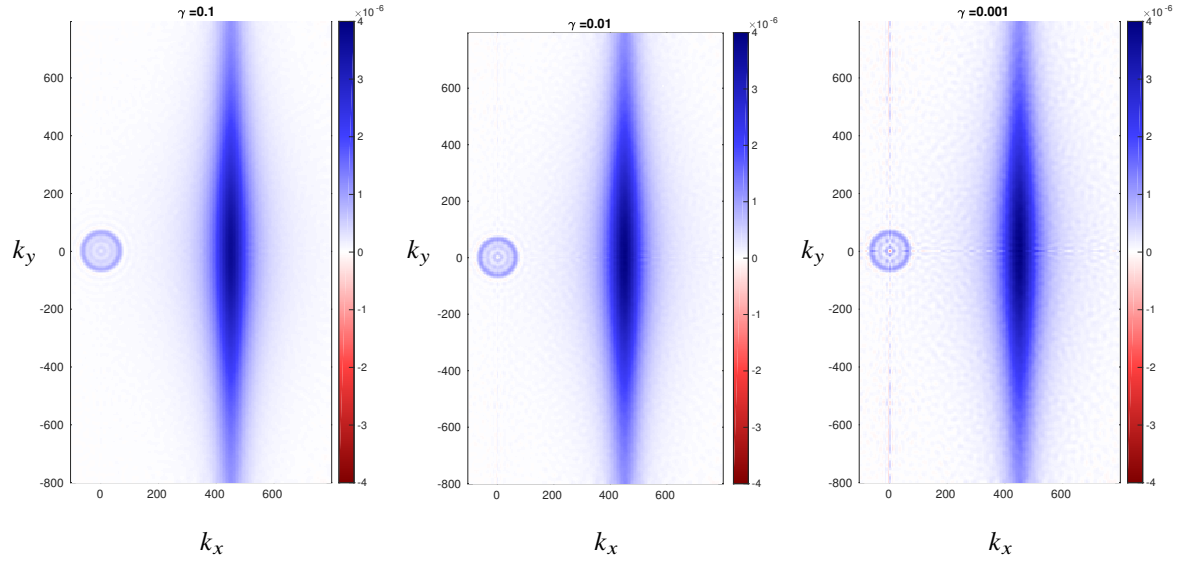

(a) $\gamma = 0.1$ **(b)** $\gamma = 0.01$ **(c)** $\gamma = 0.001$

Fig. 3 Spectra deconvolved with a Wiener filter for three values of γ.

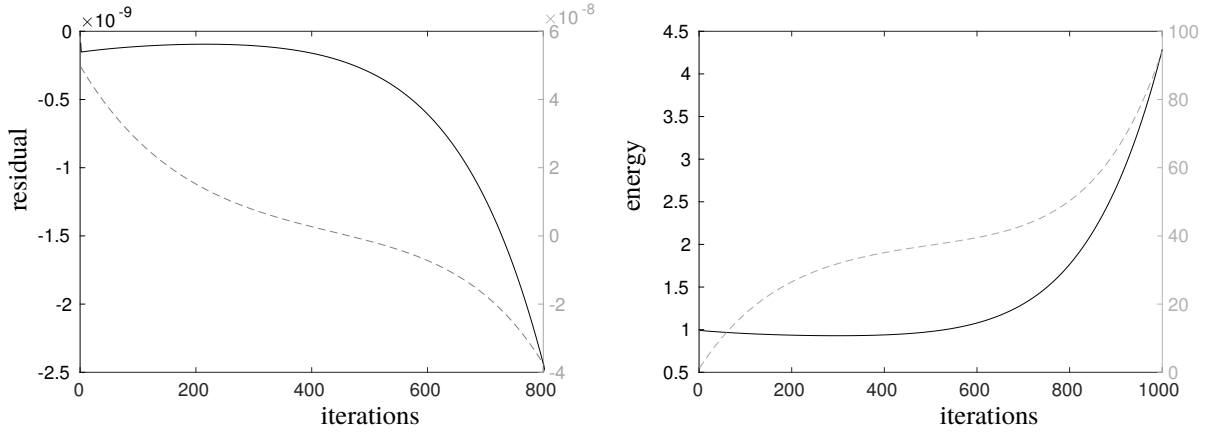

(a) residual **(b) energy /energy (original)**

Fig. 4 Residual and energy during deconvolution ——— $\tilde{h}$ normalised, – – – $\tilde{h}$ not normalised.

stable until around 500 iterations, where the amplitude of the residual indeed increases. The standard, not normalised, case does not show any stability of energy, and in fact when taking its value at 400 iterations it is more than 30 times larger than the original value. The inflection point previously discussed is thus not a suitable criteria. The presence of an extrema in the residual and a stable value of the energy indicates that $\tilde{h}$ should be normalised before implementing the deconvolution algorithm. The following results will thus be displayed for the normalised case.

Fig. 5 shows $k_y = 0$ and $k_x = k_c$ profiles of the measured spectra, before and after deconvolution, with its analytical expression for reference. As previously stated, the main effect of sampling with the antenna is the overestimation of the acoustic ridge level, and some side lobes that translate into oscillations in the profiles. The four number of iterations tested show the ability to correct for this overestimation. However, increasing the number of iterations also strengthens the oscillations, all regions of the spectra. To that regards, 200 iterations - chosen as the local minimum of residual - seem to offer a good trade-off between recovering a close enough value of the spectra at the convective ridge and keeping the oscillations' amplitude low.

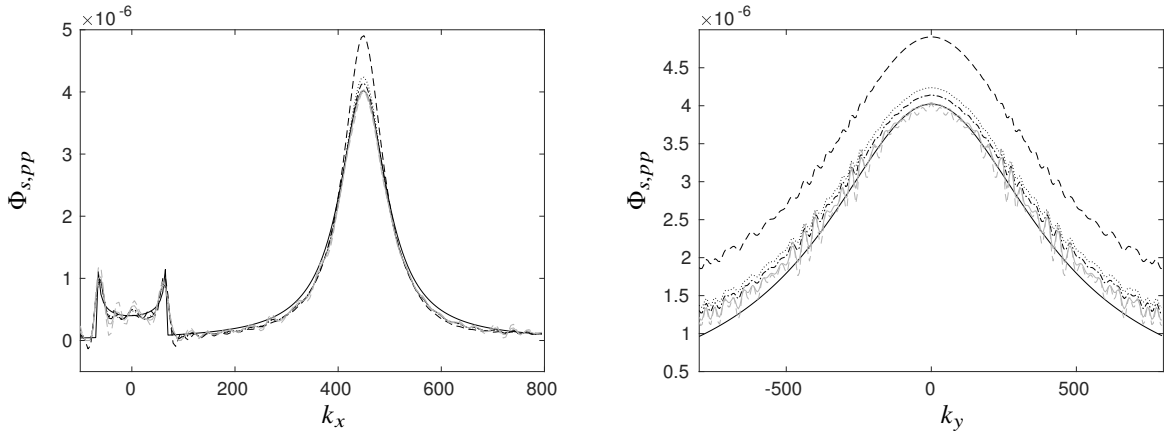

(a) $\Phi_{s,pp}$ **at** $k_y = 0$ **(b)** $\Phi_{s,pp}$ **at** $k_x = k_c$

Fig. 5 Profiles of spectra deconvolved with DAMAS2 ($\tilde{h}$ **normalised).** ——— **analytic,** − − − **array-sampled,** ····· **150 it.,** − · − · **200 it.,** ——— **300 it.,** – – – **400 it.**

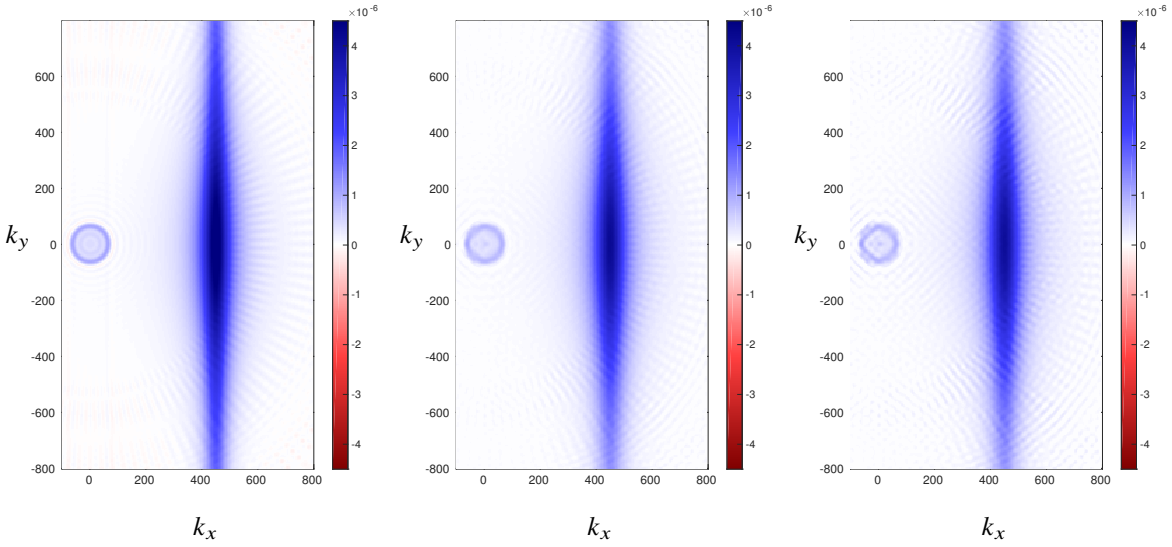

(a) Φ_{pp} **before deconvolution** **(b) 200 iterations** **(c) 300 iterations**

Fig. 6 Spectra deconvolved with DAMAS2: effect of iterations number.

The overall aspect of the spectra is visible in fig. 6 that displays the full spectra. When comparing the spectra without deconvolution (fig. 6a) and after 200 iterations (fig. 6b), one notices no striking difference. The positivity constraint of the algorithm removes the negative values, but the main effect of the deconvolution is on the levels at the convective ridge. However, when going further to 300 iterations (fig. 6c), the spectra appears more blurry which is what translates into the increased oscillations.

Filtering

The Fourier transform of a Gaussian is also a Gaussian, however, the filter Ψ is based on the norm of Υ rather than being expressed as a product of independent Gaussian on each component. Had it been the latter, both Gaussian would have transformed back to Gaussian and a straightforward interpretation of the Filter's effect on $b^{(n)}$ as a convolution would have been possible. Since the algorithm uses successive FFT (or inverse FFT) on both components, by means of

the Matlab® fft2 and ifft2 functions, this approach is not possible.

In the original description of the DAMAS2 algorithm by Dougherty [10], the Gaussian filter has one parameter (Υ_0) setting its width, which effect is thus investigated. Fig. 7 shows the residual and energy during the deconvolution with different values of Υ_0 expressed in terms of the value Υ_{Nyq} of the Nyquist criteria when performing the direct Fourier transform of the wavenumber spectra in the DAMAS2 algorithm.

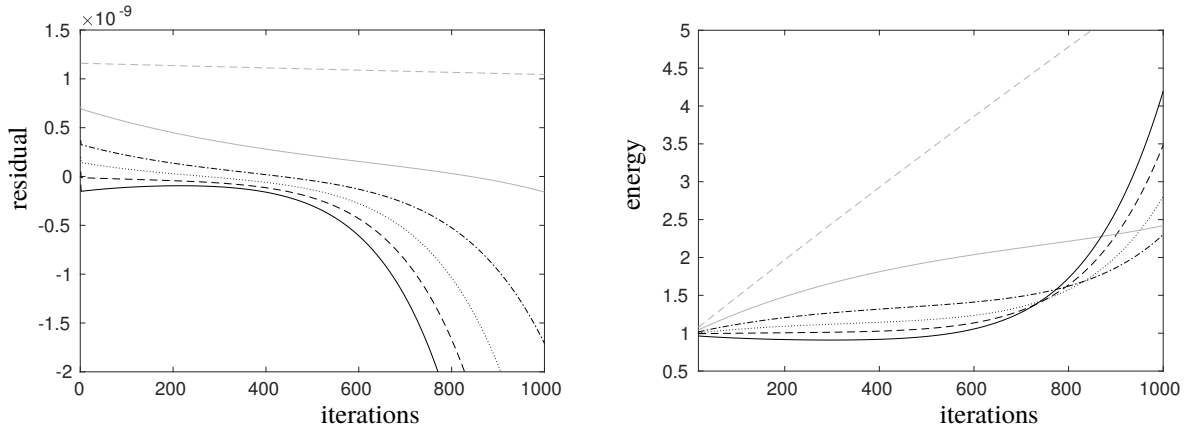

(a) residual **(b) energy /energy (original)**

Fig. 7 Residual and energy during deconvolution with various filters. ——— no filter, − − − $\Upsilon_0 = 3\Upsilon_{Nyq}$, ····· $\Upsilon_0 = 2\Upsilon_{Nyq}$, − · − · $\Upsilon_0 = 1.5\Upsilon_{Nyq}$, ——— $\Upsilon_0 = 1\Upsilon_{Nyq}$, − − − $\Upsilon_0 = 0.5\Upsilon_{Nyq}$.

It is clear from fig. 7a that only a wide filter could display a local minimum, with the $\Upsilon_0 = 3\Upsilon_{Nyq}$ tending to the previously discussed case without filter. A similar conclusion is drawn from fig. 7b, on which only the widest filter offers a stable value of energy in the output. In terms of criteria that can be tracked during the deconvolution, filtering does not seem appropriate. However, it is worth looking at the spectra before reaching a final conclusion on the matter.

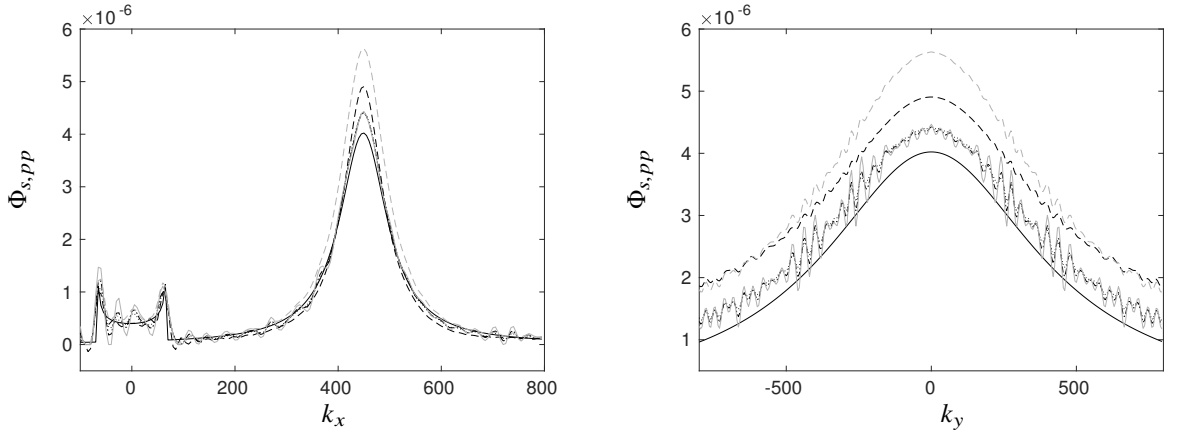

(a) $\Phi_{s,pp}$ **at** $k_y = 0$ **(b)** $\Phi_{s,pp}$ **at** $k_x = k_c$

Fig. 8 Profiles of spectra deconvolved with DAMAS2: effect of filtering. ——— analytic, − − − array-sampled, ····· $\Upsilon_0 = 3\Upsilon_{Nyq}$ /300 it., − · − · $\Upsilon_0 = 3\Upsilon_{Nyq}$ /400 it., ——— $\Upsilon_0 = 3\Upsilon_{Nyq}$ /500 it., − − − $\Upsilon_0 = 1.5\Upsilon_{Nyq}$ /300 it.

Fig. 8 shows the $k_y = 0$ and $k_x = k_c$ profiles after deconvolution for two values of filter width and different number of iterations. The two widths are selected from fig. 7 as the best width displayed and an intermediate one. In the case of $\Upsilon_0 = 3\Upsilon_{Nyq}$, one notices that despite taking a relatively large number of iterations, slightly beyond what could be taken to locally minimise the residual, the deconvolution fails to recover the value of the spectra at the convective ridge.

Increasing the number of iterations from 300 to 500 indeed strengthens the oscillations but does not improve the overall fit. The output of a narrower filter is also displayed for illustration, and shows a significant overestimate of the convective ridge.

Overall, it seems that no filter width is appropriate for this study, and that only an infinitely wide one would work, which corresponds to the case without filtering.

Tiana-Roig and Jacobsen [8] noted that the use of the Gaussian filter to remove the effect of high wavenumber (Υ-space in our case) contribution was mainly relevant for sources outside of the beam-forming source region. They explained that in their case all sources were covered by their sources region, so that the filter was not relevant any more. In our case, the use of a Gaussian filter might not be of interest either.

Positivity constraint

The final point that needs addressing in the deconvolution algorithm itself is the positivity constraint. Dougherty [10] had devised the DAMAS2 algorithm for application to sound sources power maps. Negative values in the output would thus be non-physical in that frame; however, there is no such physical argument for the current application to wavenumber-frequency spectra that can reach negative values. This section thus looks into the use of the algorithm without the positivity constraint.

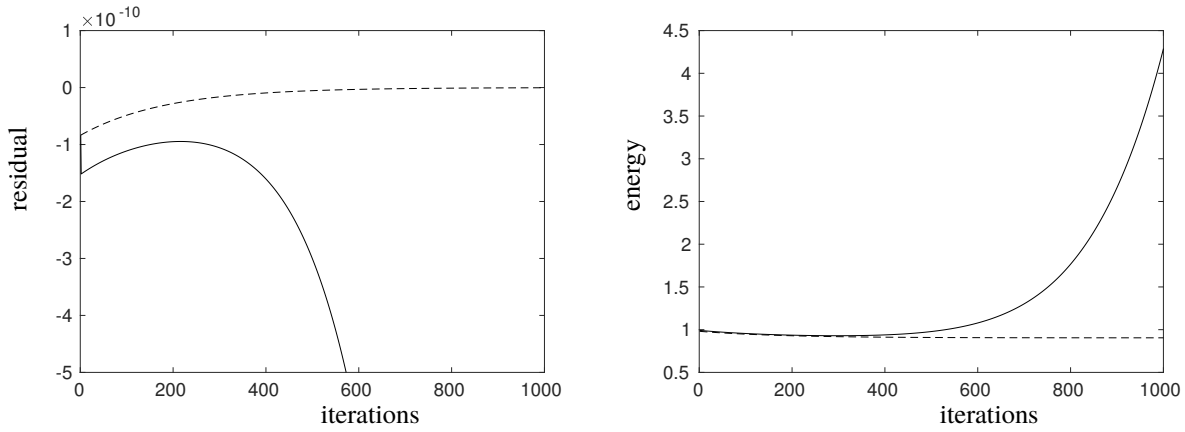

(a) residual **(b) energy /energy (original)**

Fig. 9 Residual and energy during deconvolution with and without positivity constraint (h normalised). ——— with positivity constraint, − − − without positivity constraint.

Fig. 9 shows the residual and energy during the deconvolution with and without positivity constraint. Contrary to the previous case, deconvolution with no positivity constraint does not exhibit a local minima of the residual but rather slowly tends towards zero. The energy has a similar behaviour, with a slow decay with initial values, up to 300 iterations, being close to the previously observed one. This would indicate that after a certain number of iterations the process would be stable. However, this is not the case as can be noticed by checking the spectra after various number of iterations.

Fig. 10 shows the spectrum before deconvolution, and after 200 and 500 iterations, without the positivity constraint. The number of 500 iterations corresponds to a rough estimate of when the residual could be considered converged from fig. 9a, and 200 iterations offer an intermediate check. Even after only 200 iterations, the spectra is clearly blurred compared to the original one, and after 500, it is clear that the process has diverged.

Contrary to what could have been expected from tracking the energy or residual, and despite the lack of a physical argument, the deconvolution without positivity constraint is thus not stable in the present case.

Irisation from discrete polar angle

In order to match experimental work from Salze *et al.* [5, 6], the previous test cases have been conducted with a $\pi/64$ angular resolution for the antenna. The spectra clearly displays side lobes imputable to the antenna geometry and parameters, and this even after deconvolution. It is expected that more refined angular steps should lead to their related

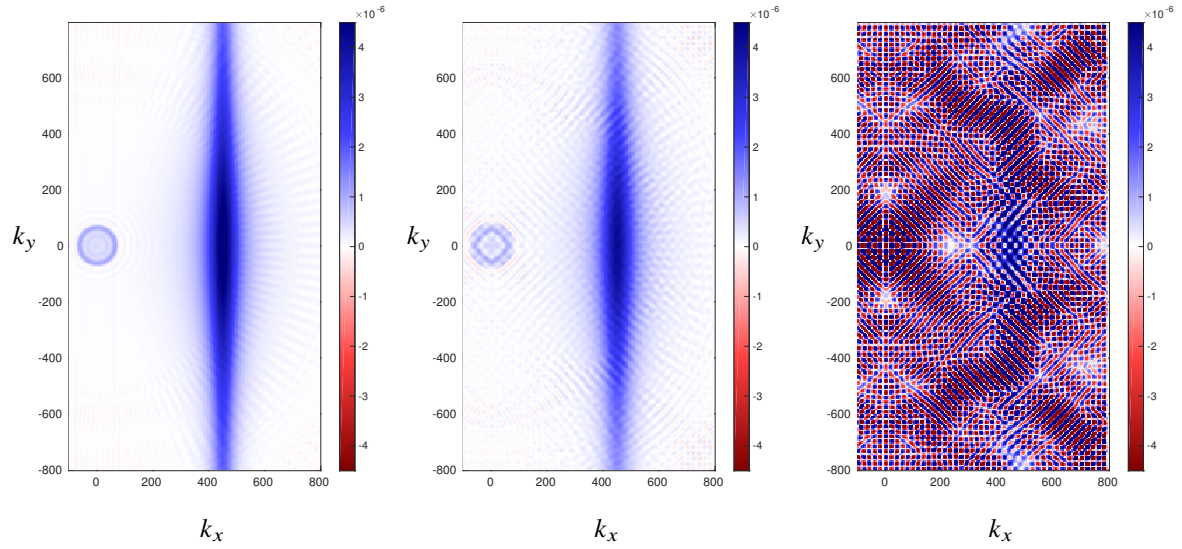

(a) Φ_{pp} **calculated from synthetic data** **(b)** Φ_{pp} **deconvolved (200it), no positivity constraint** **(c)** Φ_{pp} **deconvolved (500it), no positivity constraint**

Fig. 10 Testing positivity constraint

lobes being pushed to higher wavenumber values. The effect of the antenna's angular resolution is thus investigated in this section.

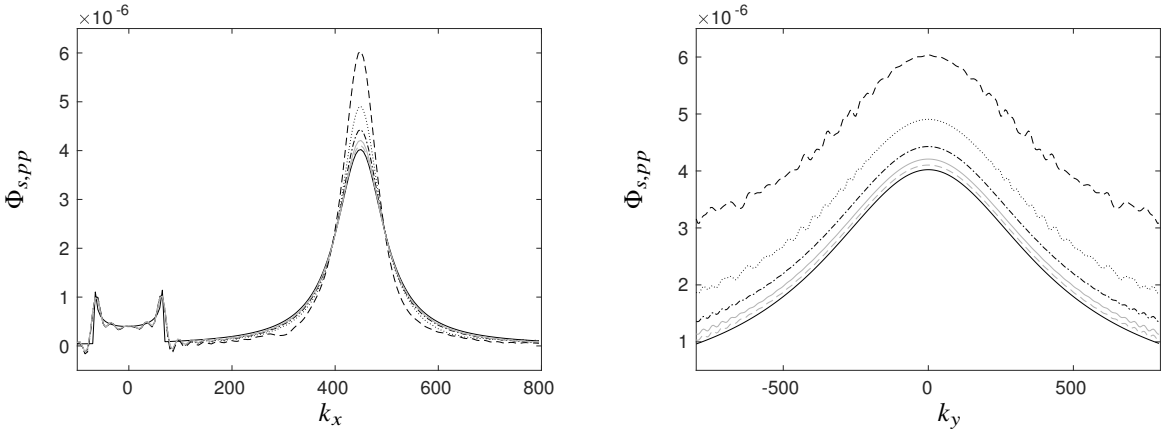

(a) $\Phi_{s,pp}$ **at** $k_y = 0$ **(b)** $\Phi_{s,pp}$ **at** $k_x = k_c$

Fig. 11 Profiles of the spectra before deconvolution for different angular resolutions. ——— **analytic,** − − − $\pi/32$**,** ····· $\pi/64$**,** − · − · $\pi/127$**,** ——— $\pi/253$**,** – – – $\pi/505$**.**

The profiles of the spectra calculated with $\pi/32$, $\pi/64$, $\pi/127$, $\pi/253$ and $\pi/505$ angular resolutions are displayed in fig. 11. One should note the results are displayed before any form of deconvolution. The $\pi/32$ calculation overestimates the value of the spectra by about 50 % in the convective part, for both $k_y = 0$ and $k_x = k_c$. The overestimate appears to be halved with each increase in the resolution. The angular resolution do not change the results for the acoustic region. However, in the sub-convective region that is about $100 < |k_x| < 350$ m^{-1} , the $\pi/32$ case differs from the others. This region being of interest for studies on fluid - structures interactions [17] gives another reason why the $\pi/32$ resolution is not enough. On the other hand, a $\pi/64$ resolution recovers the values of the spectra almost as well as the more refined cases. To that regards, $\pi/64$ can be used as the first acceptable resolution.

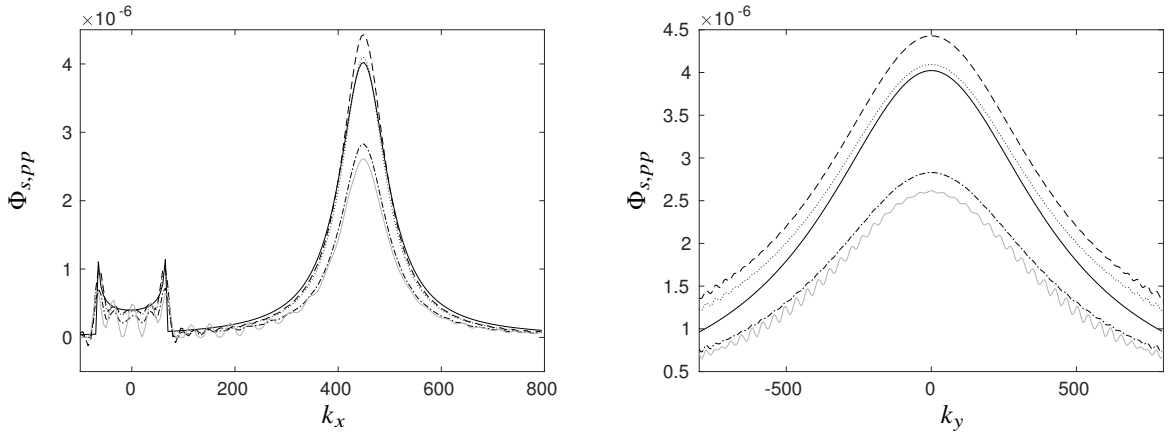

(a) $\Phi_{s,pp}$ **at** $k_y = 0$ **(b)** $\Phi_{s,pp}$ **at** $k_x = k_c$

Fig. 12 Profiles of the spectra deconvolved with DAMAS2 with a refined angular resolution (127 steps). ——— analytic, − − − array-sampled, ····· 10 it., − · − · 100 it., ——— 200 it.

Fig. 11b shows oscillations in the $k_x = k_c$ profile for $200 < |k_y| < 600$ m^{-1} that disappear for $\pi/127$ and higher resolutions. While $\pi/64$ is reasonable, it thus appears interesting to use a resolution of $\pi/127$ or finer.

Previous test cases have shown that the use of deconvolution could prove itself useful in correcting the convective ridge overestimate. Fig. 12 shows profile before and after deconvolution for the $\pi/127$ case. A few iterations seem to suffice in rendering a good estimation of the spectra, with the values for 10 iterations showing a good fit to the analytical curves. However, using the previous criteria and following the residual during the deconvolution would lead to selecting 100 to 200 iterations, which clearly is too many and deteriorate the data. In this case the use of deconvolution is thus challenging since a blind approach, that is without comparison to the analytic expression, could lead to erroneous quantitative interpretations.

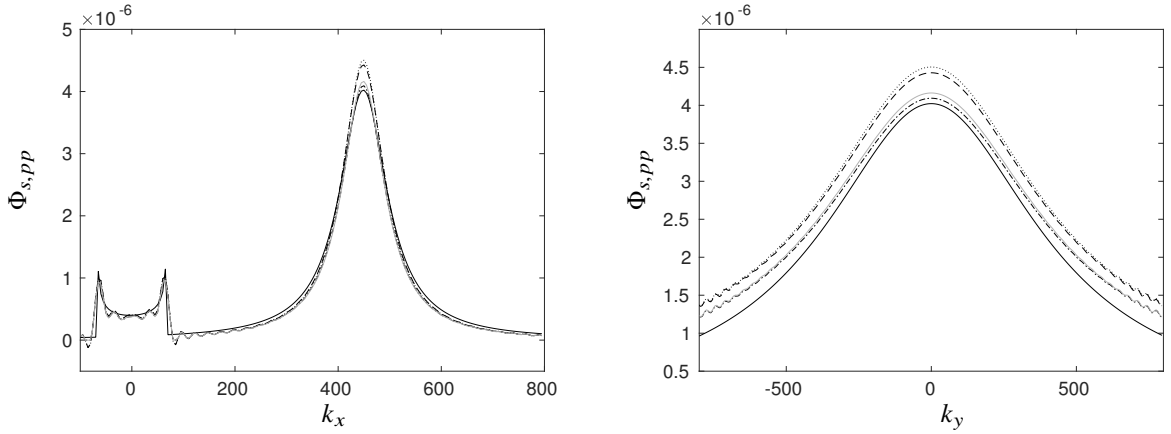

(a) $\Phi_{s,pp}$ **at** $k_y = 0$ **(b)** $\Phi_{s,pp}$ **at** $k_x = k_c$

Fig. 13 Profiles of the spectra deconvolved with DAMAS2 with 127 steps and 64 interpolated to 127. ——— $\pi/64$, − − − interp. $\pi/127$ ····· $\pi/64$ 100 it., − · − · interp. $\pi/127$ 100 it.

The use of a refined angular resolution seems nevertheless interesting. Given that the experimental campaigns the current study is referring to [5, 6] were conducted with a $\pi/64$ angular resolution, an interpolation is worth testing. Fig. 13 shows $\Phi_{s,pp}$ profiles for two cases ; first the synthetic data was sampled with a $\pi/127$ resolution with the antenna's geometry as previously presented. Secondly, the data was sampled with a $\pi/64$ resolution and interpolated to $\pi/127$. There does not seem to be a significant difference between the two cases, which indicates that experimental

data array-sampled with a $\pi/64$ resolution could be first interpolation before deconvolution. With the bettered angular resolution, the convective ridge overestimate is reduced and the effect of deconvolution should be lesser than before. Without a better criteria, an arbitrary value of 10 iterations seems a good complementary approach.

To conclude on this part, a hybrid approach of angular interpolation and a limited number of deconvolution iterations appears to reduce the convective ridge overestimate and reduce the side lobes in the regions of interest while not deteriorating the sampled data in the acoustic region.

Effect of frequency

All previous test cases were conducted at a frequency of 3700 Hz. Fig. 14 shows the residual during deconvolution for various frequencies. Although all cases display a local minimum around 195-235 iterations, it seems useful to use this curve for each case in order to apply only the required number of iterations.

Fig.15 shows $k_y = 0$ profiles of $\Phi_{s,pp}$ after deconvolution for different frequencies, the number of iterations being based on fig.14. At low frequency (500 hz) the deconvolution does not seem beneficial, since both analytic and array-sampled spectra have similar levels in the convective ridge. However, when increasing the frequency, one notices a clear discrepancy between these two values, and the deconvolution brings the spectra closer to analytic levels. At 1 kHz, the acoustic region is not well recovered, but starting from 2 kHz and higher, spectra show the two spikes corresponding to the acoustic wavenumber and the overall levels are well fitted despite some noticeable oscillations, as previously discussed.

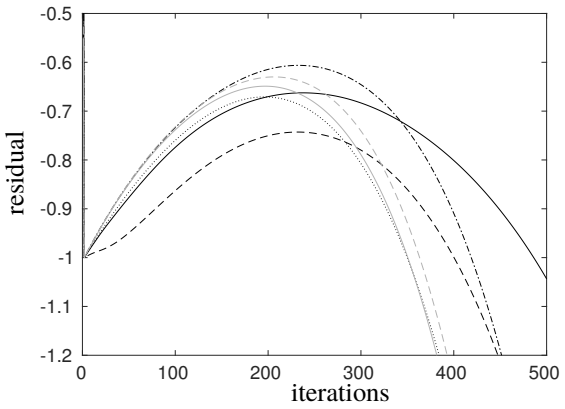

Fig. 14 Residual during DAMAS2 interations, with various frequencies. ——— 500 **Hz,** − − − 1 **kHz,** · · · · · · 2 **kHz,** − · − · 3 **kHz,** ——— 4 **kHz,** – – – 5 **kHz.**

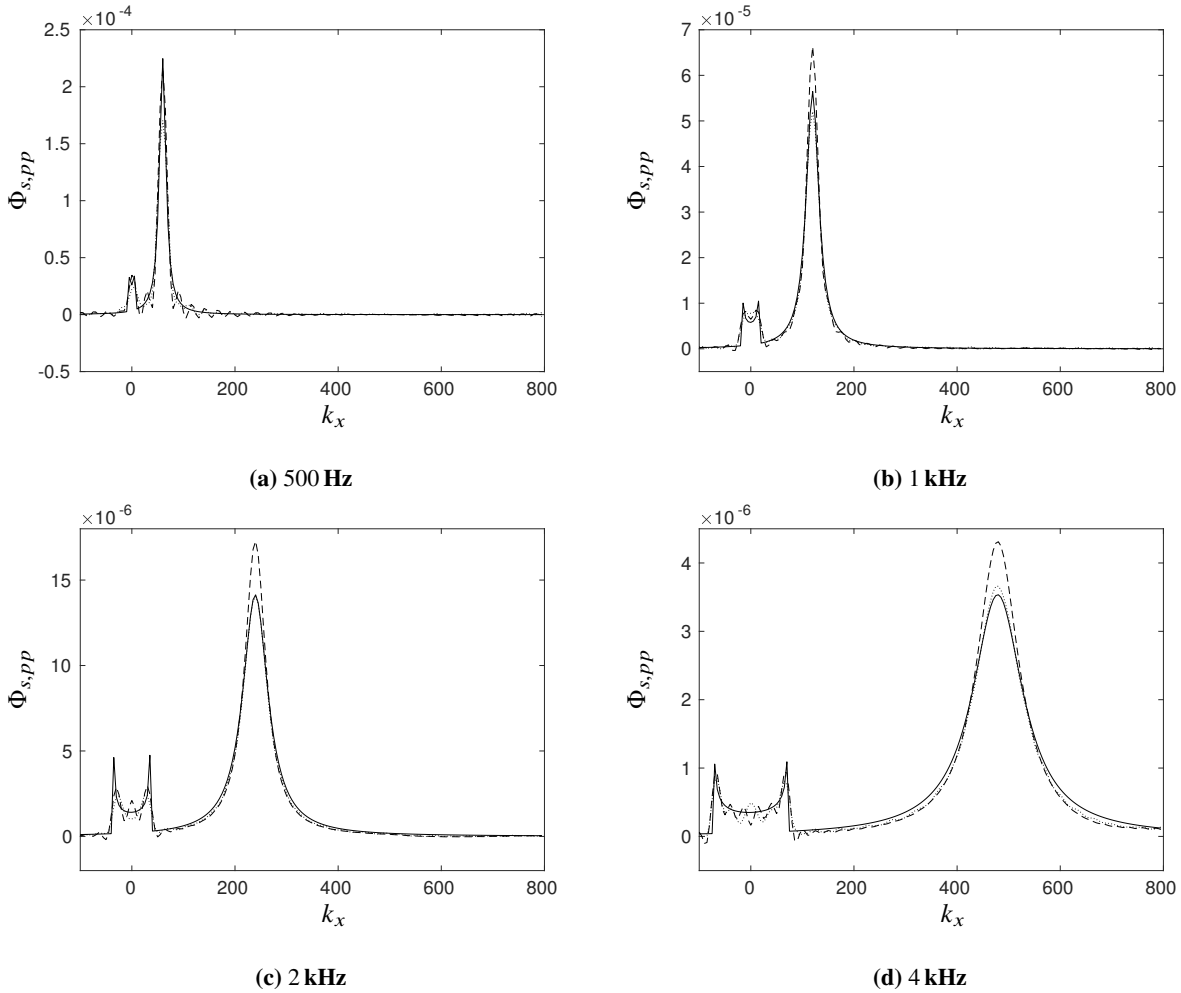

(a) 500 **Hz** **(b)** 1 **kHz**

(c) 2 **kHz** **(d)** 4 **kHz**

Fig. 15 Profiles of $\Phi_{s,pp}$ deconvolved with DAMAS2 at various frequencies. ——— analytic, − − − array-sampled, ····· deconvolved.

Application to experimental data.

Data sets from previous experimental campaigns are used to test the applicability of the discussed methods. Wall pressure measurements were conducted, within the SONOBL project, in a test section designed to create a zero pressure gradient boundary layer, placed in the anechoic chamber of the Centre Acoustique of Ecole Centrale de Lyon . A rotating antenna of 63 microphones placed in line sampled the data with a $\pi/64$ angular resolution. Further details on the set-up can be found in the studies by Salze *et al.* [5, 6]. The following is taken at 3750 Hz for the zero pressure gradient case at 75 m/s.

Two approaches are tested; in the first one, the data sampled with a $\pi/64$ resolution is deconvolved following the steps discussed previously. A second approach is to interpolate the data to a $\pi/127$ resolution, then to proceed to the deconvolution. The evolution of the residual during the deconvolution is provided in fig. 16a for both cases. It is clear that in both cases, this criteria gives a value of 100 iterations of the DAMAS algorithm. However, fig 16b shows that 100 is too many iterations for the interpolated case. For the $\pi/64$ case, a slight reduction is observed in the convective ridge, with lower but similar values to that obtained when interpolating to $\pi/127$. This is in fact similar to the point discussed with analytical test cases, and it seems that using deconvolution with the $\pi/127$ resolution would be challenging in terms of finding a criteria to stop the iterations.

The spectra for the four discussed cases are displayed in fig. 17. Applying the deconvolution to the $\pi/64$ case does not significantly alter the appearance of the spectra, appart from the negative values being removed, since the main effect is on the level of the convective ridge, as illustrated in fig 16b. However, interpolation from $\pi/64$ to $\pi/127$ reduces the

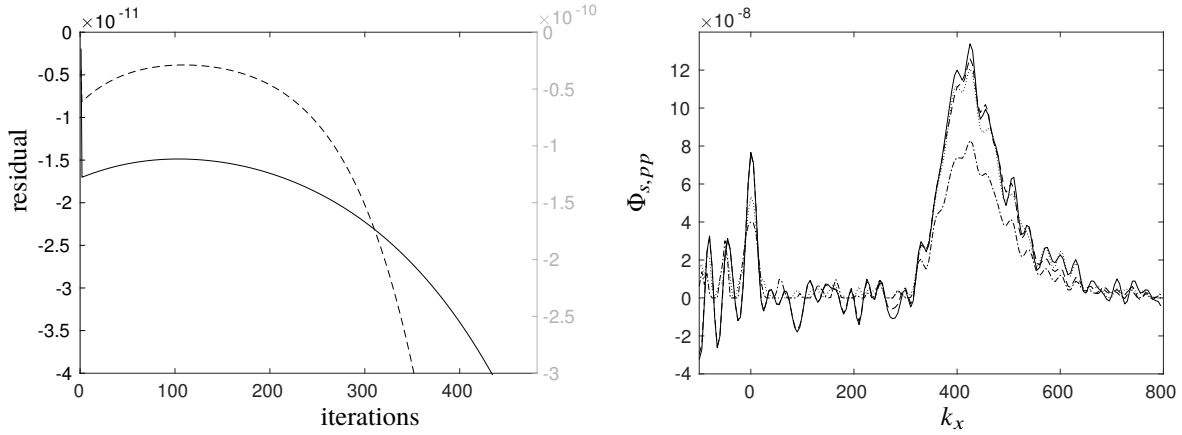

(a) Residual during deconvolution **(b) $\Phi_{s,pp}$ at $k_y = 0$**

Fig. 16 Experimental data with and without angular interpolation: (a) residual during deconvolution ——— $\pi/64$, – – – interp. $\pi/127$, and (b) $k_y = 0$ profiles of $\Phi_{s,pp}$, before and after deconvolution (b). ——— $\pi/64$, – – – interp. $\pi/127$ ····· $\pi/64$ 100 it., – · – · interp. $\pi/127$ 100 it.

side lobes in the spectra, and generally renders a smoother appearance. As noted for the analytical test cases, the side lobes visible in the convective ridge for $k_y \sim 300\,\mathrm{m}^{-1}$ disappear with the refined angular resolution.

Overall, the DAMAS2 algorithm appears to behave similarly on the experimental data as it does on the analytical test cases previously conducted.

Conclusion

Analytical test cases are used to assess the applicability of the Wiener filter and DAMAS2 deconvolution methods to the wavenumber-frequency spectra of wall pressure turbulence beneath a turbulent boundary layer. Within the frame of this study, the array used to sample the data is a rotating antenna developed in previous studies, with 63 lined microphones and an angular resolution of $\pi/64$.

While the Wiener filter method has the clear advantage of not being iterative and therefore not raising the question of when to stop the algorithm, its output displays significant oscillations, in particular in the acoustic region. The DAMAS2 algorithm has been tested and its different parameters investigated. For the purpose of this study, it appears that the transfer function of the antenna should be normalised by its Frobenius norm to offer stability of the output's energy. No Gaussian filter should be applied during the iteration process, and although there is a lack of a physical argument for it, the positivity constraint is necessary during this process. With these notes, the DAMAS2 algorithm offers a means to correcting the observed overestimate of the spectra in the convective region, that is inputed to the antenna's geometry. However, it has little effect on the side lobes that translate into oscillations in $k_y = 0$ or $k_x = k_c$ profiles. These side lobes are essentially due to the coarse angular resolution of the rotating antenna, and are indeed reduced when refining this resolution. The main limitation is found in that the criteria for convergence of the DAMAS2 iterative process does not hold when refining the angular resolution, either by interpolating between angular positions or by directly re-sampling synthetic data with a finer rotation.

In lights of the present study, and until a more reliable criteria for convergence is defined, it seems better to use an angular interpolation, or a hybrid approach with a few steps of interpolation.

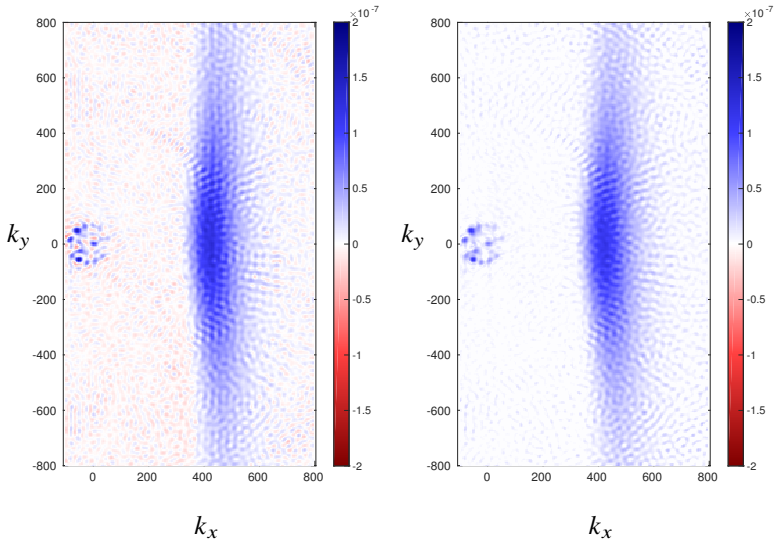

(a) Φ_{pp} $\pi/64$ **(b)** Φ_{pp} $\pi/64$**, DAMAS2 100 it.**

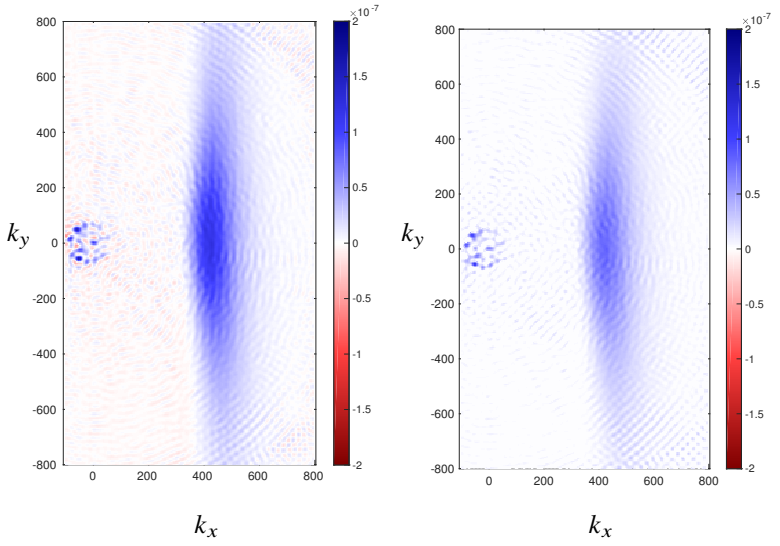

(c) Φ_{pp} **interp. to** $\pi/127$ **(d)** Φ_{pp} **interp. to** $\pi/127$**, DAMAS2 100 it.**

Fig. 17 Spectra from experimental data, before and after deconvolution.

Acknowledgement

This research has been funded by the European Union through the CANOBLE Cleansky project (H2020-CS2-CFP02-2015-01, project id 717084), and by the Labex CeLyA of Université de Lyon, operated by the French National Research Agency (ANR-10-LABX-0060/ ANR-11-IDEX-0007).

References

[1] Bull, M. K., "Wall-pressure fluctuations beneath turbulent boundary layers: Some reflections on forty years of research," *Journal of Sound and Vibration*, Vol. 190, No. 3, 1996, pp. 299–315. doi:10.1006/jsvi.1996.0066.

[2] Willmarth, W. W., "Pressure Fluctuations Beneath Turbulent Boundary Layers," *Annual Review of Fluid Mechanics*, Vol. 7, No. 1, 1975, pp. 13–36. doi:10.1146/annurev.fl.07.010175.000305.

[3] Corcos, G. M., "Resolution of Pressure in Turbulence," *The Journal of the Acoustical Society of America*, Vol. 35, No. 2, 1963, pp. 192–199. doi:10.1121/1.1918431.

[4] Arguillat, B., Ricot, D., Bailly, C., and Robert, G., "Measured wavenumber: Frequency spectrum associated with acoustic and aerodynamic wall pressure fluctuations," *The Journal of the Acoustical Society of America*, Vol. 128, No. 4, 2010, pp. 1647–1655. doi:10.1121/1.3478780.

[5] Salze, É., Bailly, C., Marsden, O., Jondeau, E., and Juvé, D., "An experimental characterisation of wall pressure wavevector-frequency spectra in the presence of pressure gradients," *20th AIAA/CEAS Aeroacoustics Conference*, 2014, p. 2909.

[6] Salze, É., Bailly, C., Marsden, O., Jondeau, E., and Juvé, D., "An experimental investigation of wall pressure fluctuations beneath pressure gradients," *21st AIAA/CEAS Aeroacoustics Conference*, 2015, p. 3148.

[7] Ehrenfried, K., and Koop, L., "Comparison of Iterative Deconvolution Algorithms for the Mapping of Acoustic Sources," *AIAA Journal*, Vol. 45, No. 7, 2007. doi:10.2514/1.26320.

[8] Tiana-Roig, E., and Jacobsen, F., "Deconvolution for the localization of sound sources using a circular microphone array." *The Journal of the Acoustical Society of America*, Vol. 134, No. 3, 2013, pp. 2078–89. doi:10.1121/1.4816545.

[9] Lylloff, O., Fernández-Grande, E., Agerkvist, F., Hald, J., Tiana Roig, E., and Andersen, M. S., "Improving the efficiency of deconvolution algorithms for sound source localization," *The Journal of the Acoustical Society of America*, Vol. 138, No. 1, 2015, pp. 172–180. doi:10.1121/1.4922516.

[10] Dougherty, R., "Extensions of DAMAS and benefits and limitations of deconvolution in beamforming," *11th AIAA/CEAS aeroacoustics conference*, 2005, p. 2961.

[11] Bahr, C. J., and Cattafesta, L. N., "Wavenumber-frequency deconvolution of aeroacoustic microphone phased array data of arbitrary coherence," *Journal of Sound and Vibration*, Vol. 382, 2016, pp. 13–42. doi:10.1016/j.jsv.2016.06.044.

[12] Haxter, S., and Spehr, C., "Infinite beamforming: wavenumber decomposition of surface pressure fluctuations," *Proceedings of the 5th Berlin Beamforming Conference*, 2014, pp. 1–10.

[13] Ehrenfried, K., and Koop, L., "Experimental study of pressure fluctuations beneath a compressible turbulent boundary layer," *14th AIAA/CEAS AeroAcoustics Conference*, Vol. 57, 2008.

[14] Gonzalez, R. C., and Woods, R. E., *Digital Image Processing*, second edi ed., 2002. doi:10.1007/3-540-27563-0.

[15] Brooks, T. F., and Humphreys, W. M., "A deconvolution approach for the mapping of acoustic sources (DAMAS) determined from phased microphone arrays," *Journal of Sound and Vibration*, Vol. 294, No. 4, 2006, pp. 856–879. doi:10.1016/j.jsv.2005.12.046.

[16] Brooks, T., and Humphreys, W., "Extension of DAMAS phased array processing for spatial coherence determination (DAMAS-C)," *12th AIAA/CEAS Aeroacoustics Conference (27th AIAA Aeroacoustics Conference)*, 2006, p. 2654.

[17] Maxit, L., "Simulation of the pressure field beneath a turbulent boundary layer using realizations of uncorrelated wall plane waves," *The Journal of the Acoustical Society of America*, Vol. 140, No. 2, 2016, pp. 1268–1285.